Scattering from a truncated von Neumann–Wigner potential

T. A. Weber and D. L. Pursey
Department of Physics and Astronomy, Iowa State University, Ames, Iowa 50011-3160
(Received 26 November 1997)

In 1929, von Neumann and Wigner [Phys. Z. **30**, 465 (1929)] demonstrated the existence of local potentials which support a bound state with energy embedded in the continuous spectrum. In this paper, we study the s-wave scattering produced by a class of von Neumann–Wigner potentials which are perturbed by truncating them at some large radius $r=a$. For the class of potentials considered, we obtain an analytic expression for the Jost function. The original continuum bound state is replaced by a well isolated complex zero of the Jost function (equivalent to a pole of the S matrix), but this does not produce a conventional Breit-Wigner resonance. Instead, we find twin peaks in the cross section, separated by a very narrow gap associated with the Jost function zero. Our study continues with an account of bound states and virtual states supported by the potential, and with an investigation of the form of asymptotically large zeros of the Jost function. We compare the results of this paper with the significantly different results we obtained using a different perturbation [Phys. Rev. A **52**, 3932 (1995)]. [S1050-2947(98)02005-8]

PACS number(s): 03.65.Nk, 03.80.+r

I. INTRODUCTION

Local potentials that support bound states with positive energy embedded in the continuous spectrum (''continuum bound states'') were first constructed by von Neumann and Wigner [1]. Recently, interest in this topic was renewed because of two experimental developments. The first was the reported observation of narrow positron-electron coincidence peaks in heavy ion collisions [2]. In an attempt to understand these, two groups [3,4] independently performed detailed numerical calculations for the electron-positron system using relativistic two-body approximations related to the Bethe-Salpeter equation. The American and the Russian groups both found numerical evidence for the existence of continuum bound states in this system, and suggested that the experimentally observed peaks might be a reflection of such states. To the best of our knowledge, these theoretical calculations have not been definitively refuted, although the experimental evidence for the peaks remains controversial. In the second experimental development, Capasso *et al.* [5] carefully constructed a superlattice consisting of ultrathin semiconductor layers for which they report the remarkable observation of an electronic bound state with no classical turning points. The potential consists of a series of barriers all of the same height. Infrared absorption measurements revealed a narrow isolated transition from a bound state within a quantum well formed by the barriers to a bound state greater than the barrier height. Because the barrier heights are all the same, this problem is easily amenable to theoretical analysis [6].

Thus continuum bound states or close relatives thereof have been observed by Capasso *et al.*, are predicted by some calculations to exist in the electron-positron system, and might possibly have been observed in the latter system. However, a bound state cannot be observed unless it interacts with some other system, and such an interaction must perturb the bound state, in general converting it into a state of finite width. For the semiconductor heterostructure studied by Capasso *et al.*, the sharp ''zero width'' state is perturbed by the radiation field and by the necessary cutoff demanded by the finite size of the sample. For the electron-positron case, one would like to establish a clear experimental signal for the existence of the continuum bound states. To attempt this in the context of the full numerical computations of Refs. [3,4] would be a daunting (if desirable) task. However, Arbuzov *et al.* [7] have developed a quasilocal approximation to their electron-positron interaction that, although energy-dependent, shares some of the characteristics of a von Neumann–Wigner potential. We [8], and independently Zastavenko [9] using a different approach, have argued that this approximate quasilocal potential cannot support continuum bound states of the energy needed to explain the results of the full numerical calculation. Nevertheless, this approximation suggests that results obtained by studying perturbed von Neumann–Wigner systems may have relevance for the much more complicated relativistic electron-positron problem, as well as for nonrelativisitc systems. This provides the motivation for the present paper.

The goal of this paper, as well as that of our earlier work [10], is to study the s-wave scattering produced by perturbations of a particular class of von Neumann–Wigner potentials. The particular von Neumann–Wigner potentials that we perturb, and the particular perturbations that we consider, are chosen to allow a completely analytic treatment of the Jost function. This strategy produces a clarity of insight that may be lost in a more numerical approach or in an approach based on perturbation theory, but at the cost of some separation from realistic experimental situations. The present studies suggest some of the phenomena to be expected in a more realistic but inevitably less analytic calculation.

In order to study the Jost function, we need not only the bound state solution but the scattering solutions as well. For this reason, we consider only the subset of von Neumann–Wigner continuum bound states that were obtained in Ref. [11] using a particular class of degenerate Gel'fand-Levitan equations. This subset was also obtained by Pappademos *et al.* [12] using the techniques of supersymmetric quantum

mechanics and by Stahlhofen [13] using a variation of the Darboux transformation [14].

In Ref. [10] we radially shifted a class of von Neumann–Wigner potentials. Under such a shift, solutions to the s-wave radial Schrödinger equation at the energy of the unperturbed continuum bound state are no longer able to satisfy the boundary conditions both at infinity and at the origin. Thus, neither a bound state nor a scattering state exists at that energy. For a small enough shift, the Jost function has a zero in the lower half complex k plane near the real axis, which produces a typical resonance in the cross section. As the shift parameter goes to zero, this Jost function zero approaches the real k axis, in the limit giving a ''resonance'' of zero width, that is, a continuum bound state.

In the present paper we perturb the same class of von Neumann–Wigner potentials by introducing a cutoff, thus producing a potential of finite range. The Jost function possesses a well isolated zero near the wave number of the unperturbed continuum bound state. However, the scattering cross section does not exhibit a conventional resonance. Instead of a single peak in the cross section, we find two closely spaced peaks, separated by a very narrow gap in which the cross section drops strictly to zero. Further investigation shows that it is the narrow gap between the peaks rather than the peaks themselves that is associated with the Jost function zero. This turns out to be an extreme form of the Ramsauer-Townsend effect, in which the ''resonance'' phenomenon is well approximated by an *inverted* Breit-Wigner shape. In Appendix A we sketch a treatment of resonance phenomena, including the extreme Ramsauer-Townsend effect, as background for the main thrust of this paper.

In the following section we introduce the potentials and solutions of the Schrödinger equation for a class of von Neumann–Wigner potentials that support a continuum bound state with energy $E_0=k_0^2$. In Sec. III we determine the Jost function for the scattering when this potential is truncated. In Sec. IV we treat the comparatively simple case in which the cutoff point is chosen at a zero of the von Neumann–Wigner potential. This special case illustrates most of the ''resonance'' phenomena. We return to the general case in Sec. V, which among other things illustrates how the phenomena change with small changes in the cutoff. Some technical details are relegated to Appendix B. This leads in Sec. VI to a discussion of Levinson's theorem, conventional bound states, and imaginary zeros of the Jost function. Again, technical details are presented in Appendix C. In Sec. VII we study the asymptotic form of large complex zeros of the Jost function, and show it to agree with the Regge estimate [15]. We compare the present results with those of Ref. [10] in Sec. VIII. In a concluding section we comment on our results.

II. THE VON NEUMANN–WIGNER POTENTIAL AND SOLUTIONS

Throughout this paper we use units in which $\hbar=1$ and $2m=1$. For simplicity we confine our attention to the case of the radial Schrödinger equation for zero angular momentum,

$$\left[-\frac{d^2}{dr^2}+V(r)\right]\psi(r)=k^2\psi(r), \quad 0\leqslant r<\infty. \tag{1}$$

The energy eigenvalue is $E=k^2$. We deal only with potentials that are less singular than $1/r$ at the origin and that vanish at infinity, so that physically acceptable solutions must vanish at $r=0$ and be bounded as $r\to\infty$. We begin with the Schrödinger equation for a free particle, $V(r)=0$, and use the Gel'fand-Levitan equation to insert a bound state with energy $E_0=k_0^2$ into the continuous spectrum. This procedure creates a new Schrödinger equation with a potential belonging to a subset of von Neumann–Wigner potentials. The reader is referred to our earlier papers [11] for the technical details: here we merely quote the results, which can be directly verified by substitution into the Schrödinger equation. This method provides explicit expressions for the scattering states as well as for the continuum bound state, and therefore allows for a completely analytical discussion of the scattering theory.

The resulting von Neumann–Wigner potential is

$$V_{\text{vN-W}}(r)=-\frac{8k_0^2\sin 2k_0r}{2k_0r+\lambda-\sin 2k_0r}+\frac{8k_0^2(1-\cos 2k_0r)^2}{(2k_0r+\lambda-\sin 2k_0r)^2}, \tag{2}$$

where λ is a positive constant related to the normalization of the bound state. If $\lambda>3.889$, the continuum bound state energy is greater than the maximum of the potential: thus while a quantum particle of energy E_0 is bound, a classical particle with the same energy would have no classical turning points and must escape the potential [16].

The regular solution with energy $E=k^2$ for the Schrödinger equation with the potential given by Eq. (3), normalized so that the wave function and its first derivative evaluated at the origin are 0 and 1, respectively, is

$$\varphi(r,k)=u(r,k)-\frac{u(r,k_0)s(r,k)}{\lambda+s(r,k_0)}, \tag{3}$$

where

$$u(r,k)=\frac{1}{k}\sin kr \tag{4}$$

is the regular solution for the free particle,

$$s(r,k)=\frac{2k_0^2}{k}\left\{\frac{\sin[(k-k_0)r]}{k-k_0}-\frac{\sin[(k+k_0)r]}{k+k_0}\right\}, \tag{5}$$

and in particular

$$s(r,k_0)=2k_0r-\sin 2k_0r. \tag{6}$$

For $k=k_0$, the solution reduces to

$$\varphi(r,k_0)=\frac{\lambda u(r,k_0)}{\lambda+s(r,k_0)}, \tag{7}$$

which is normalizable. Therefore $\varphi(r,k_0)$ represents the bound state with positive energy $E_0=k_0^2$ embedded in the continuous spectrum.

III. THE JOST FUNCTION AND SCATTERING PHASE SHIFTS

In this paper we study the s-wave scattering for the truncated potential

$$V_{\text{cutoff}}(r)=\begin{cases} V_{\text{vN-W}}(r), & r\leqslant a \\ 0, & r>a, \end{cases} \tag{8}$$

where $V_{\text{vN-W}}(r)$ was defined in Eq. (2). We use $\psi(r,k)$ to denote the regular solution with energy $E=k^2$ to the Schrödinger equation with the potential $V_{\text{cutoff}}(r)$. This solution may be written as

$$\psi(r,k)=\begin{cases} \varphi(r,k), & r\leqslant a \\ (2ik)^{-1}\{\mathfrak{F}_-(k,a)e^{ikr}-\mathfrak{F}_+(k,a)e^{-ikr}\}, & r\geqslant a, \end{cases} \tag{9}$$

where the Jost function

$$\mathfrak{F}(k,a)\equiv\mathfrak{F}_+(k,a)=\mathfrak{F}_-^*(k^*,a)=e^{ika}[\varphi'(a,k)-ik\varphi(a,k)] \tag{10}$$

is found by matching the two forms of $\psi(r,k)$ and their first derivatives at $r=a$. The prime in Eq. (10) denotes differentiation with respect to a.

From Eqs. (5) and (10) we find

$$\mathfrak{F}(k,a)=1-\frac{e^{ika}}{\lambda+s(a,k_0)}\{s(a,k)[\cos k_0a-iku(a,k_0)] +4k_0^3[u(a,k_0)]^2\varphi(a,k)\}. \tag{11}$$

For $k\to\infty$, $\mathfrak{F}(k,a)\to 1$ as expected. The Jost function for such a finite range potential is known to be an entire function of k with at most a finite number of zeros on the positive imaginary k axis, no other zeros in the upper half complex k plane, and an infinite number of zeros in the lower half plane [17]. Zeros on the positive imaginary k axis, if they exist at all, correspond to bound states. Zeros in the lower half plane may correspond to resonances provided they are sufficiently isolated and are near the real k axis [18]. The limit of the Jost function as $a\to\infty$ is not uniform in k, since

$$\lim_{a\to\infty}\mathfrak{F}(k,a)=1, \quad k\neq k_0, \tag{12}$$

while

$$\lim_{a\to\infty}\mathfrak{F}(k_0,a)=0. \tag{13}$$

For all values of k, however, the S-matrix element given by

$$S(k,a)=\frac{\mathfrak{F}^*(k,a)}{\mathfrak{F}(k,a)}=e^{2i\delta(k,a)} \tag{14}$$

has the limit 1 as $a\to\infty$. Here $\delta(k,a)$ is the s-wave scattering phase shift.

IV. A SPECIAL CASE

The analysis is much simpler when

$$k_0a=n\pi, \tag{15}$$

where n is an integer, for then $u(a,k_0)=0$. These values of k_0a also correspond to zeros of the oscillating potential. Then from Eqs. (4), (5), and (11) we find that

$$\mathfrak{F}(k,a)=1-e^{ika}\frac{4k_0^3\sin ka}{k(k^2-k_0^2)(\lambda+2k_0a)}. \tag{16}$$

We anticipate that the perturbation of the system due to the truncation of the von Neumann–Wigner potential will replace the continuum bound state by a well isolated complex zero of the Jost function close to $k=k_0\equiv n\pi/a$. We estimate its position be assuming $|(k-k_0)a|\ll 1$ and expanding $\mathfrak{F}(k,a)$ in powers of $(k-k_0)a$. This yields

$$\mathfrak{F}(k,a)=\frac{1}{\lambda+2k_0a}[\lambda-(k-k_0)a(2ik_0a-3)] +O((k-k_0)^2a^2), \tag{17}$$

which gives

$$k=K_n\equiv k_0-\frac{3\lambda}{4k_0^2a^3}-i\frac{\lambda}{2k_0a^2} \tag{18}$$

for the location of the zero closest to k. (The notation K_n indicates that this zero is near $k=k_0=n\pi/a$.) This zero is well isolated in the sense defined in Appendix A, and can be placed arbitrarily close to the real axis by taking a sufficiently large. The approximation $|ka-n\pi|\ll\pi$ used to derive Eq. (18) is valid provided $\lambda\ll 2k_0a=2n\pi$. If $k_0a\gg 1$, then $|\mathrm{Re}(K_n-k_0)|\ll|\mathrm{Im}K_n|$, so that the wave number k_0 associated with the original continuum bound state lies well within the width of the ''resonance'' region associated with the zero K_n.

Naively one would expect this well isolated zero to be associated with a conventional resonance in the scattering cross section, but this is false. Equation (16) shows that $\mathfrak{F}(k,a)$ is real at $k=k_0=n\pi/a$, so that the phase shift is zero at this wave number. As already noted, this falls well within the expected Breit-Wigner peak centered on $\mathrm{Re}K_n$. Thus the resonance phenomenon associated with the zero K_n of the Jost function is not a Breit-Wigner peak: instead it is very close to the ''inverted Breit-Wigner'' form discussed in Appendix A. As k increases through $k=k_0$, the phase shift increases rapidly from near $-\pi/2$ to near $+\pi/2$, never reaching $+\pi/2$ and reaching $-\pi/2$ only if $\lambda\lesssim 27/(16n\pi)$. We relegate the details to Appendix B.

We illustrate these findings by studying $\sin^2\delta(k,a)$, which is more convenient than studying the s-wave partial cross section $\sigma(k,a)=(4\pi/k^2)\sin^2\delta(k,a)$, since the unitarity limit is given by $\sin^2\delta(k,a)=1$. From Eq. (14),

$$\sin^2\delta(k,a)=\frac{1}{4}\left|\frac{\mathfrak{F}(k,a)-\mathfrak{F}^*(k,a)}{\mathfrak{F}(k,a)}\right|^2. \tag{19}$$

Equation (16) then yields

$$\sin^2\,\delta(k,a) = \frac{4\sin^4 ka}{\left[ka\left(1-\frac{k^2}{k_0^2}\right)\left(1+\frac{\lambda}{2k_0a}\right)+\sin 2ka\right]^2+4\sin^4 ka}. \tag{20}$$

The cross section vanishes whenever $ka=m\pi$, where m is an integer, while the intervening peaks are of varying heights and typically have a width at half maximum somewhat smaller than $\pi/2a$. The two peaks between $(n-1)\pi$ and $(n+1)\pi$ are particularly large and appear as twin peaks separated by a very narrow gap as the cross section drops precipitously to zero at $k=k_0=n\pi/a$. This is illustrated in Fig. 1(a) for $n=5$ and $\lambda=1$. The gash separating the twin peaks is due to the ''resonance pole'' at $k=K_n$, as is shown by the dramatic increase of the phase shift as k increases through the gap region, illustrated in Fig. 1(b). The exact $\sin^2(k,a)$ is compared to the ''pole approximation'' of Eq. (A11) in Fig. 1(c), using the approximation of Eq. (18) for the complex zero of the Jost function. We attribute the minor discrepancies in the width and the position of the zero in Fig. 1(c) to the approximation $|(k-k_0)a|\ll 1$ used to derive Eq. (18). For the example of Fig. 1, $\delta_{\rm nr}(k,a)\approx\arctan(10\pi/3)=0.470\pi$, so that the resonance structure is very close to that of an inverted Breit-Wigner. This becomes especially apparent when Fig. 1(c) is viewed upside down.

Figure 1(a) also shows a prominent peak for small values of k. We discuss this further in the next section and in Sec. VI.

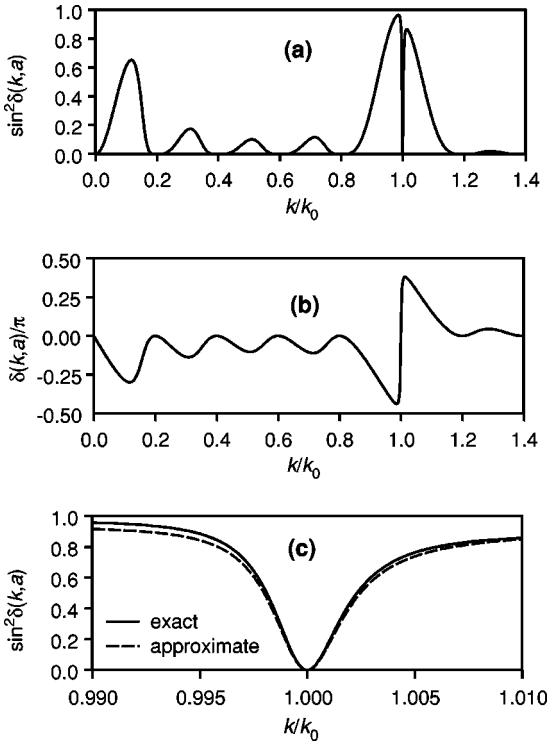

FIG. 1. $\sin^2\delta(k,a)$ and $\delta(k,a)$ plotted against k/k_0 for $\lambda=1$ and $k_0a=5\pi$. (a) $\sin^2\delta(k,a)$. Note the resonance structure near $k=k_0$ and the broad peak near $k=0.1k_0$. (b) $\delta(k,a)$. Note the rapid increase of $\delta(k,a)$ from near $-\pi/2$ to near $+\pi/2$ coinciding in position with the dramatic dip in $\sin^2\delta(k,a)$ near $k=k_0$. (c) Detail of $\sin^2\delta(k,a)$ near $k=k_0$ compared with the ''pole approximation'' of Eq. (A11), using the approximation of Eq. (18) for the zero K_n of the Jost function.

V. THE GENERAL CASE

We now return to the general Jost function given by Eq. (11). Before proceeding, it is convenient to introduce the following new notations. We define b and β (where $0\leqslant\beta<\pi$) by

$$b\equiv k_0a\equiv n\pi+\beta, \tag{21}$$

and we define a dimensionless wave number variable z by

$$z\equiv k/k_0. \tag{22}$$

We rewrite Eq. (11) as

$$\mathfrak{F}(k,a)=X+iY, \tag{23}$$

where after some work we find

$$X=1+\frac{2z\,\sin 2\beta\,\cos 2bz-2\cos 2\beta\,\sin 2bz}{z(z^2-1)(\lambda+2b-\sin 2\beta)}+\frac{2[\sin 2\beta\,\sin 2bz-z(1-\cos 2\beta)(1+\cos 2bz)](1-\cos 2\beta)}{z(z^2-1)(\lambda+2b-\sin 2\beta)^2} \tag{24}$$

and

$$Y=-\frac{2(1-\cos 2bz)\cos 2\beta-2z\sin 2\beta\,\sin 2bz+2z^2(1-\cos 2\beta)}{z(z^2-1)(\lambda+2b-\sin 2\beta)} +\frac{2[(1-\cos 2bz)\sin 2\beta-z(1-\cos 2\beta)\sin 2bz](1-\cos 2\beta)}{z(z^2-1)(\lambda+2b-\sin 2\beta)^2}. \tag{25}$$

For z (or equivalently k) real, X and Y are $\mathrm{Re}\mathfrak{F}(k,a)$ and $\mathrm{Im}\mathfrak{F}(k,a)$, respectively.

The obvious question arises whether the ''inverted Breit-Wigner'' structure in the cross section persists for arbitrary values of the cutoff, or whether it is a feature unique to the special case considered in the preceding section. We attack this question first by seeking a complex zero of $\mathfrak{F}(k,a)$ near $k=k_0$, and then seeking a real zero of $\mathrm{Im}\mathfrak{F}(k,a)$ near $k=k_0$. If such a zero exists and is well inside the expected ''resonance peak'' associated with the complex zero of $\mathfrak{F}(k,a)$, then (as in Appendix A) we expect to find a structure in the cross section similar to an ''inverted Breit-Wigner'' shape.

For the complex zero of $\mathfrak{F}(k,a)$ near $k=k_0$ we expand both X and Y in powers of $(z-1)$, keeping only the constant and first order terms. We assume that $b\gg 1$, and that λ may also be large. Therefore we retain only those terms of highest order in b and λ except when these terms have coefficients that may be small or zero for certain values of β. In this way we find the approximate zero of $\mathfrak{F}(k,a)\equiv X+iY$ to be

$$K_n \approx k_0 - \frac{\lambda(1+2\cos^2 2\beta)}{4k_0^2a^3} - i\frac{\lambda}{2k_0a^2} + O\left(\frac{\lambda}{k_0^3a^4}\right). \quad (26)$$

If $\beta=0$ (corresponding to $b\equiv k_0a=n\pi$) this reduces to Eq. (18), as it should. The approximations leading to Eq. (26) are valid provided $|K_n/k_0-1|\ll b^{-1}$, which is true provided $\lambda \ll 2b=2k_0a$. We conclude that the Jost function possesses a complex zero close to k_0, which may be expected to generate resonance phenomena.

Using the same approximations, we find

$$\mathrm{Im}\mathfrak{F}(k_1,a)=0$$

with

$$k_1 \approx k_0 - \frac{\lambda(1-\cos 2\beta)^2}{2k_0a^2(\lambda+2k_0a)} + O\left(\frac{\lambda}{k_0^3a^4}\right). \quad (27)$$

With $\lambda \ll 2b$, necessary for the validity of Eq. (26), and with $b\gg 1$,

$$|k_1-\mathrm{Re}K_n| \approx \frac{\lambda(2+\cos 2\beta)|\cos 2\beta|}{4k_0^2a^3} \ll |\mathrm{Im}K_n|. \quad (28)$$

Hence $\mathrm{Im}\mathfrak{F}(k,a)=0$ [and therefore $\delta(k,a)=0$] at a wave number k_1 well inside the ''resonance region'' of width $2|\mathrm{Im}K_n|$ centered on $\mathrm{Re}K_n$. We conclude that the cross section will display a structure near $k=k_0$ similar to an inverted Breit-Wigner structure, except possibly when λ is comparable in size to or larger than $b=k_0a$.

These results are illustrated in Fig. 2. The typical behavior of $\sin^2\delta(k,a)$ when β is not necessarily zero is illustrated in Fig. 2(a). The cross section is qualitatively similar to that for $\beta=0$, illustrated in Fig. 1, with a strong peak at low momentum and a strong twin peak near $k=k_0$ separated by a narrow gap associated with the resonance pole. However, the pattern of intermediate peaks is less regular and somewhat modified.

For the case $\beta=\pi/2$ illustrated in Fig. 2(a), the strong low momentum peak reaches the unitarity limit $\sin^2\delta(k,a)=1$.

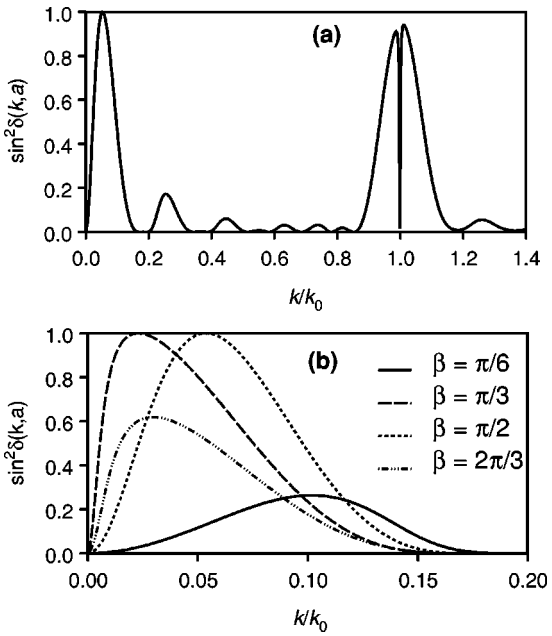

FIG. 2. $\sin^2\delta(k,a)$ plotted against k/k_0 for $\lambda=1$ and $k_0a=5\pi+\beta$. (a) $\sin^2\delta(k,a)$ for $\beta=\pi/2$. Note the resonant structure near $k=k_0$. (b) Detail of $\sin^2\delta(k,a)$ for $0\leqslant k<k_0$, for several values of β. The peak near $k=0.1k_0$ for $\beta=0$, shown in Fig. 1(a), decreases in height as β increases and practically disappears when $\beta=\pi/4$ (not plotted). A new peak which reaches the unitarity limit $\sin^2\delta(k,a)=1$ has appeared closer to the origin when $\beta=\pi/3$. As β increases beyond $\pi/2$, this peak moves to smaller k values, and shrinks below the unitarity limit.

The growth and eventual decay of this peak as β increases from $\pi/6$ through $2\pi/3$ is illustrated in Fig. 2(b). This peak is due to an imaginary zero of the Jost function, associated either with a virtual state or with a very weakly bound state, depending on the value of β. We discuss this in detail in the next section.

VI. LEVINSON'S THEOREM AND IMAGINARY ZEROS OF THE JOST FUNCTION

In this section we shall gain a better understanding of the low momentum peaks in Figs. 1 and 2 through studying possible bound or virtual states. We begin by considering Levinson's theorem.

The potential $V_{\mathrm{cutoff}}(r)$ defined in Eq. (8) satisfies all of the conditions for the validity of Levinson's theorem. Therefore,

$$\delta(0,a)-\delta(\infty,a)=N_b\pi, \quad (29)$$

where N_b is the number of bound states. From Eqs. (23)–(25) we see that

$$\mathfrak{F}(\infty,a)=1 \quad (30)$$

and

$$\mathfrak{F}(0,a)=\text{real}. \quad (31)$$

Since

$$\mathfrak{F}(k,a)=|\mathfrak{F}(k,a)|e^{-i\delta(k,a)}, \quad (32)$$

we conclude that N_b in Eq. (29) is even (or zero) if $\mathfrak{F}(0,a)>0$ and odd if $\mathfrak{F}(0,a)<0$. Since the unperturbed potential $V_{\text{vN-W}}(r)$ does not support any conventional bound states, we do not expect many bound states for the perturbed system. We therefore assume $N_b \leqslant 1$, interpreting $\mathfrak{F}(0,a)>0$ as implying no bound states and $\mathfrak{F}(0,a)<0$ as implying one bound state. These interpretations will be confirmed later in the section, when we discuss imaginary zeros of the Jost function.

From Eq. (24) we find

$$\mathfrak{F}(0,a)=\frac{F(\lambda,b,\beta)}{(\lambda+2b-\sin 2\beta)^2}, \tag{33}$$

where

$$\begin{aligned}F(\lambda,b,\beta)=\lambda^2+4[b(1+\cos 2\beta)-\sin 2\beta]\lambda \\ +4b^2(1+2\cos 2\beta)-12b\ \sin 2\beta \\ +(1-\cos 2\beta)(7-\cos 2\beta).\end{aligned} \tag{34}$$

This quadratic in λ is positive, and therefore $\mathfrak{F}(0,a)>0$, except for $\lambda_- \leqslant \lambda \leqslant \lambda_+$, where

$$\begin{aligned}\lambda_\pm = 2\sin 2\beta - 2b(1+\cos 2\beta) \\ \pm[4b^2\cos^2 2\beta + 4b(1-2\cos 2\beta)\sin 2\beta \\ +(5\cos 2\beta-3)(1-\cos 2\beta)]^{1/2}.\end{aligned} \tag{35}$$

Hence for most values of λ there will be no bound states, but for $\lambda_- < \lambda < \lambda_+$ there will be one bound state. In particular, the existence of a bound state requires that λ_+ be real and positive. The $\lambda_\pm$ will be real if the expression in square brackets in Eq. (35) is positive. If this is true, then λ_+ will be positive if either $b<\tan\beta$ or $4b^2(1+2\cos 2\beta) - 12b\ \sin 2\beta + (1-\cos 2\beta)(7-\cos 2\beta) < 0$. With $b=n\pi+\beta$, as in Eq. (21), we find from more detailed analysis that $\lambda_+>0$ for $n=1$ only if $0.2824\pi<\beta<0.6128\pi$. These lower and upper bounds for β approach $\pi/3$ and $2\pi/3$, respectively, as $n\to\infty$. In summary, Levinson's theorem shows that the potential $V_{\text{cutoff}}(r)$ with cutoff $a\equiv(n\pi+\beta)/k_0 \geqslant \pi/k_0$ supports a bound state for a finite range $\sup(\lambda_-,0)<\lambda<\lambda_+$ of the parameter λ, provided β is within a range $\beta_-(n)<\beta<\beta_+(n)$, where $0.2824\pi<\beta_-(n)<\pi/3$ and $0.6128\pi<\beta_+(n)<2\pi/3$.

For the examples illustrated in Fig. 2(b) with $b=5\pi+\beta$, the $\lambda_\pm$ are complex only if $0.70\pi \leqslant \beta \leqslant 0.78\pi$, which does not include any of the illustrated values of β. Equation (35) shows that $\lambda_+<0$ for $b=5\pi+\beta$ and $\beta=\pi/6$ or $\beta=2\pi/3$: hence there are no bound states for these values of b and β, and the corresponding curves in Fig. 2(b) do not reach the unitarity limit $\sin^2\delta(k,a)=1$. However, $\lambda_+>0$ for the cases $\beta=\pi/3$ and $\beta=\pi/2$, and a bound state may be present if $\lambda<\lambda_+$. Numerical computation shows that $\lambda_+=4.69$ for $\beta=\pi/3$ and $\lambda_+=34.33$ for $\beta=\pi/2$. Since the cases plotted for $\beta=\pi/3$ and $\beta=\pi/2$ in Fig. 2(b) have $\lambda=1<\lambda_+$, they possess bound states and the corresponding curves reach the unitarity limit as expected.

We confirm these results by considering the imaginary zeros of the Jost function. To seek such zeros, we first set

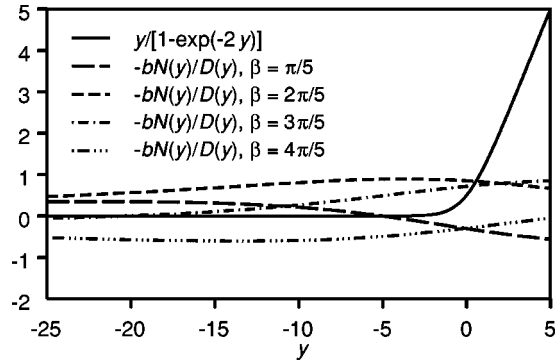

FIG. 3. Imaginary zeros $k=iy/a$ of $\mathfrak{F}(k,a)$ are given by intersections of the curves $-bN(y)/D(y)$ and $y/(1-e^{-2y})$. The negative root of Eq. (36) when $\beta=\pi/5$ moves along the y axis as β increases, and has become positive when $\beta=2\pi/5$. This root reaches a maximum near $y=0.79$ when $\beta\approx\pi/2$ (not illustrated) and then begins to retreat as β continues to increase, while a second negative root moves along the y axis from $-\infty$. Eventually the two roots coincide and move onto the complex y plane, as has already happened when $\beta=4\pi/5$.

$$ka=iy. \tag{36}$$

The condition $\mathfrak{F}(k,a)=0$ may then be manipulated into the form

$$f(y)\equiv\frac{y}{1-e^{-2y}}=-\frac{bN(y)}{D(y)}, \tag{37}$$

where

$$\begin{aligned}N(y)=\frac{(\lambda+2b)\cos 2\beta-\sin 2\beta}{\lambda+2b-\sin 2\beta} \\ +\frac{y}{b}\left(\frac{(\lambda+2b)\sin 2\beta-2(1-\cos 2\beta)}{\lambda+2b-\sin 2\beta}\right)\end{aligned} \tag{38}$$

and

$$\begin{aligned}D(y)=\frac{2(1-\cos 2\beta)^2}{\lambda+2b-\sin 2\beta}-\sin 2\beta-\frac{y}{b}(1-\cos 2\beta) \\ +\frac{1}{2}\left[1+\left(\frac{y}{b}\right)^2\right](\lambda+2b-\sin 2\beta).\end{aligned} \tag{39}$$

Here we give only a descriptive account of the roots of Eq. (37). The analytic justification for our description is provided in Appendix C. Equation (37) develops a real root at $y=-\infty$ when $\beta=0$. As β increases, this root migrates along the y axis (equivalently, up the imaginary k axis) and becomes positive for β somewhat less than $\pi/3$. It continues to increase with increasing β, reaching a maximum close to 0.8 for a value of β a little less than $\pi/2$. As β continues to increase, the positive root begins to move back along the y axis, while a second root starts to move along the axis from $-\infty$. Before β reaches $3\pi/4$, the two roots coincide (at a negative value), then separate again as they move onto the complex y plane (equivalently, the two imaginary roots in k space develop equal and opposite real parts). These results are illustrated in Fig. 3.

Positive imaginary zeros of the Jost function correspond to bound states, while negative imaginary zeros, if small, correspond to virtual states. Both virtual states and weakly bound states generate large zero momentum peaks in the cross section. In $\sin^2\delta(k,a)$, this is reflected by the strong peaks at low wave number, apparent in Figs. 1 and 2.

To conclude this section, we compare the energy of the bound states associated with imaginary zeros of the Jost function with the amplitude of the oscillations of the potential near the cutoff at $r=a$. We use the result $y_{\max}<0.79$ from Appendix C. For $y>0$, the bound state must have energy $E=-(y/a)^2>-0.624/a^2$. From Eq. (2), there must exist some r_0 in the range $a-\pi/2k_0\leqslant r_0\leqslant a$ such that $|V_{\text{cutoff}}(r_0)|$ is of order $4k_0/a$. Hence $|E/V_{\text{cutoff}}(r_0)|\lesssim 0.16/k_0a$. Since we are assuming that $k_0a\gg 1$, it follows that the binding energy of any bound state is very small compared to the maxima and minima of the potential near the cutoff, and tends to zero as $a\to\infty$.

VII. ASYMPTOTICALLY LARGE COMPLEX ZEROS OF THE JOST FUNCTION

The Jost function for a finite range potential has infinitely many zeros. We denote the mth zero with positive real part, counting from the zero of the real axis, by K_m. The zeros with negative real part are given by $K_{-m}=-K_m^*$. Regge [15] has shown that as $m\to\infty$ the real and imaginary parts of K_m have the asymptotic form

$$\begin{aligned}\mathrm{Re}K_m&=m\pi a^{-1}+O(1),\\ \mathrm{Im}K_m&=-\frac{1}{2}(\sigma+2)a^{-1}\ln m+O(1),\end{aligned}\tag{40}$$

where σ is defined by the behavior of the potential near the cutoff through

$$V(r)=(\text{const})(a-r)^{\sigma}+\cdots,\quad r\lesssim a.\tag{41}$$

In particular, for the potential $V_{\text{cutoff}}(r)$ defined in Eq. (8),

$$\sigma=\begin{cases}1, & V_{\text{cutoff}}(a)=0\\ 0, & V_{\text{cutoff}}(a)\neq 0,\end{cases}\tag{42}$$

where from Eq. (2), $V_{\text{cutoff}}(a)=0$ if $\tan k_0a=0$ or $\tan k_0a=\frac{1}{2}(\lambda+2k_0a)$. In this section, we find asymptotic forms for the zeros of the Jost function for the potential $V_{\text{cutoff}}(r)$, and show their agreement with Eq. (40).

We write

$$ka=z=x+iy,\tag{43}$$

and then manipulate the condition $\mathfrak{F}(k,a)=0$ into the form

$$e^{2iz}\equiv e^{-2y+2ix}=A(z),\tag{44}$$

where

$$A(z)=-\frac{1}{2B(z)}\times[i(z/b)(1-z^2/b^2)(\lambda+2b-\sin 2\beta)^2-2C(z)],\tag{45}$$

$$B(z)=(\lambda+2b)\cos 2\beta-\sin 2\beta-i(z/b)[(\lambda+2b)\sin 2\beta-2(1-\cos 2\beta)],\tag{46}$$

and

$$C(z)=(\lambda+2b)\cos 2\beta-\sin 2\beta-i(z/b)(1-\cos 2\beta)^2+(z/b)^2(\lambda+2b-\sin 2\beta)(1-\cos 2\beta).\tag{47}$$

Hence

$$y=-\frac{1}{2}\ln|A(z)|\tag{48}$$

and

$$A(z)=|A(z)|e^{2ix}.\tag{49}$$

From Eqs. (45)–(47), provided $\tan\beta\neq 0$ and $\tan\beta\neq\frac{1}{2}(\lambda+2b)$ we find the asymptotic form for $|z|\gg b$,

$$A(z)\approx-\frac{(z/b)^2(\lambda+2b-\sin 2\beta)^2}{2[(\lambda+2b)\sin 2\beta-2(1-\cos 2\beta)]}+O(z/b),\tag{50a}$$

while if $\tan\beta=0$ or $\tan\beta=\frac{1}{2}(\lambda+2b)$,

$$A(z)\approx\frac{i(z/b)^3(\lambda+2b-\sin 2\beta)^2}{2[(\lambda+2b)\cos 2\beta-\sin 2\beta]}+O(z^2/b^2).\tag{50b}$$

However, $\tan\beta=0$ or $\tan\beta=\frac{1}{2}(\lambda+2b)$ are just the conditions under which $V_{\text{cutoff}}(a)=0$. Hence

$$y=\begin{cases}-\ln|z|+O(1), & |z|\gg b,\quad V_{\text{cutoff}}(a)\neq 0\\ -\frac{3}{2}\ln|z|+O(1), & |z|\gg b,\quad V_{\text{cutoff}}(a)=0.\end{cases}\tag{51}$$

Since $\ln|z|\ll|z|$ for large $|z|$, we conclude that

$$|y|\ll|x|,\quad |z|\gg b.\tag{52}$$

Hence we approximate $z\approx x=$ real. It then follows from Eqs. (50) that the complex phase of $A(z)$ is approximately $(2m+1)\pi$ if $V_{\text{cutoff}}(a)\neq 0$ and approximately $(2m+\frac{1}{2})\pi$ if $V_{\text{cutoff}}(a)=0$. Hence the complex zeros of the Jost function have the asymptotic form

$$\mathrm{Re}K_m=ma^{-1}\pi+O(1)\tag{53a}$$

and

$$\mathrm{Im}K_m = \begin{cases} -a^{-1}\ln m + O(1), & V_{\mathrm{cutoff}}(a) \neq 0 \\ -\dfrac{3}{2}a^{-1}\ln m + O(1), & V_{\mathrm{cutoff}}(a) = 0. \end{cases} \tag{53b}$$

We see from Eqs. (40) and (42) that this agrees with the Regge prediction.

It is possible to improve on Eqs. (53) by an iteration. We have found that a first order correction δx_m, obtained from Eqs. (50) using $z_m \approx m\pi + iy_m$ with $y_m \equiv \mathrm{Im}K_m a$ obtained from Eq. (53b), together with an improved estimate for y_m found using $z_m \approx m\pi + \delta x_m$ in Eq. (48), usually yields an excellent approximation to numerically calculated zeros for $\mathrm{Re}K_m > k_0$. It is also possible to find good approximations for zeros in the range $0 < \mathrm{Re}K_m < k_0$, using a similar approach. We omit these further developments.

VIII. COMPARISON WITH PREVIOUS WORK

In our earlier paper [10], we considered the s-wave scattering due to a von Neumann–Wigner potential perturbed by shifting it radially through a small amount $\Delta r = \alpha/k_0$. In that case, the Jost function has only two zeros. If $\lambda > \sin 2\alpha + 2|\sin\alpha|$, then the real parts of the two roots are equal in magnitude but opposite in sign. If λ is significantly larger than $\sin 2\alpha + 2|\sin\alpha|$, then the root with positive real part generates a conventional Breit-Wigner resonance centered on a wave number $K = k_0[1 - (2/\lambda)\sin 2\alpha - (2/\lambda)^2 \sin^4\alpha]^{1/2}$. In contrast, the Jost function for the truncated potential has infinitely many complex zeros. None of these generates a conventional Breit-Wigner resonance, but the zero K_n, given approximately by Eq. (26), generates a dramatic resonant dip close to an inverted Breit-Wigner in shape.

We illustrate this comparison in Fig. 4. We choose parameters λ, α, and a with λ large enough for the shifted potential to produce a Breit-Wigner resonance and with α and a chosen so that the two potentials produce resonance structures of roughly equal width. Figure 4(a) compares the truncated potential with $\lambda = 7$ and $a = 5.5\pi/k_0$ to the shifted potential with the same value of λ and with $\alpha = 0.07\pi$. Figure 4(b) compares $\sin^2\delta(k)$ for the two potenials. In an experimental situation, attention would most probably be focused on the twin peak in the cross section with the truncated potential, and it might not even be possible to resolve the gash separating the peaks. Although the twin peaks are not due to a resonance, they become very narrow for a sufficiently large cutoff. Therefore, in Fig. 4(c) we compare $\sin^2\delta(k)$ for a truncated potential with $a = 30\pi/k_0$ with $\sin^2\delta(k)$ for the same shifted potential used in Figs. 4(a) and 4(b). The cutoff in Fig. 4(c) is chosen so that the combined width of the twin peaks for the truncated potential is comparable to the width of the resonant peak for the shifted potential.

Part of the difference between the two results may be attributed to the qualitative difference between the two potentials. The truncated potential is of finite range and, according to the standard analysis [17], the associated Jost function has an infinite number of zeros in the lower half complex k plane, while the Jost function for an infinite range potential might not even exist in the lower half k plane. The range of the shifted von Neumann–Wigner potential is infinite, and in Ref. [10] we showed that the Jost function for that potential has at most two zeros in the lower half plane. However, the twin peaks and the inverted Breit-Wigner resonance produced by the truncated potential are a major surprise. Our analysis shows that this structure exists for a as small as π/k_0 and persists for all greater values of the cutoff, no matter how large. More study is needed to pin down the exact cause of this phenomenon.

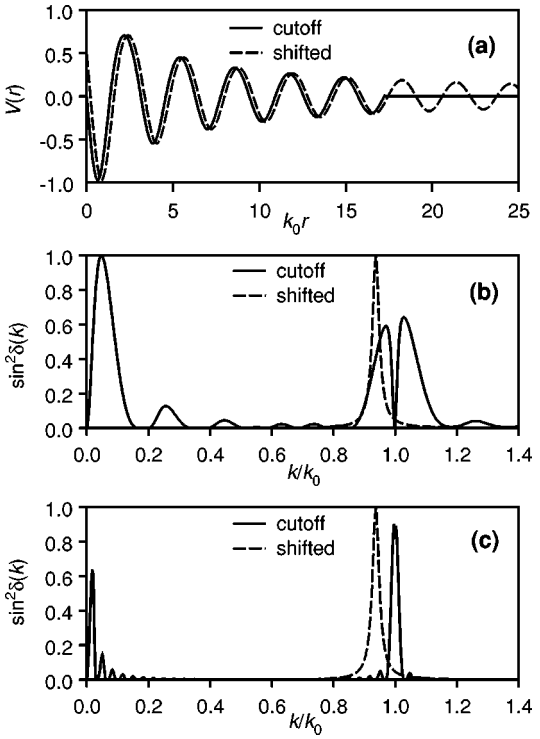

FIG. 4. Comparison of results of this study with those reported in [10]. (a) The truncated potential $V_{\mathrm{cutoff}}(r)$ of Eq. (8) with $\lambda = 7$ and $a = 5.5\pi/k_0$ compared to the shifted potential $V_{\mathrm{shifted}}(r)$ defined in Ref. [10] with $\lambda = 7$ and $\alpha = 0.07\pi$. (b) $\sin^2\delta(k)$ plotted against k/k_0 for the two potentials illustrated in (a). (c) $\sin^2\delta(k)$ plotted against k/k_0 for $V_{\mathrm{cutoff}}(r)$ with $\lambda = 7$ and $a = 30\pi/k_0$, compared to $\sin^2\delta(k)$ for the same $V_{\mathrm{shifted}}(r)$ used in (a) and (b). The large cutoff a is chosen so that the (nonresonant) split peak near $k = k_0$ has approximately the same width as the (resonant) peak due to $V_{\mathrm{shifted}}(r)$.

IX. CONCLUSION

In the usual understanding, a bound state with energy embedded in the continuum is best regarded as a resonance of zero width. If such states are of physical significance, then it is important to study how these states manifest themselves in scattering when the potential supporting them is perturbed in a variety of ways. One would hope that the perturbed system would possess a resonance that becomes the continuum bound state in the limit when the perturbation disappears. This was the case for the shifted von Neumann–Wigner potentials that we studied in Ref. [10]. In contrast to the expected results, perturbation by truncation leads to a double peak in the cross section, and it is the gap separating the peaks rather than the peaks themselves that represents resonant phenomena. While it is possible in principle for one of the twin peaks to reach the unitarity limit (although not as a

resonance), in our model this occurs only for a very limited range of the parameters. As the cutoff moves to infinity, the twin peaks become much sharper, their widths eventually shrinking to zero. As this happens, the width of the gap between them—the true resonance phenomenon—shrinks even faster than the widths of the peaks. At the same time, the twin peaks increase in height although they never quite reach the unitarity limit. Thus for sufficiently large cutoffs the gap between the peaks will not be experimentally resolvable, and the twin peaks will appear as a single peak very nearly but not quite reaching the unitarity limit. Because of limits imposed by experimental resolution, such a phenomenon could well be mistaken for a single resonance peak. In summary, for a truncated von Neumann–Wigner potential, the experimental signal for a perturbed continuum bound state is not a resonance in the scattering but pronounced twin peaks, which, if an experiment is incapable of resolving the gap separating them, might easily be mistaken for a single resonant peak.

The results reported in this paper demonstrate a flaw in the standard derivation of the Breit-Wigner formula from the unitarity of the S matrix. In the language of Appendix A, the standard assumption that $\delta_{\rm nr}(k)$ is small as well as slowly varying near the resonance pole of the S matrix is not necessarily true. We find it surprising that a seemingly innocent finite range potential, such as that studied here, should generate a Ramsauer-Townsend effect so extreme as to produce an almost perfectly *inverted* Breit-Wigner structure in the cross section. However, Dehnen and Shahin [19], studying the possible existence of magnetically quasibound positronium by using the two-body Bethe-Salpeter equation to derive an energy-dependent nonlocal effective potential, predicted a series of twin peaks in the electron-positron scattering cross section. It is not clear whether the double structure of their peaks is due to an accidental background interference [20] or is an intrinsic property of their nonlocal potential. If it is the latter, it would be most interesting to know whether their twin peaks, like ours, represent an extreme Ramsauer-Townsend phenomenon.

ACKNOWLEDGMENTS

One of the authors (T.A.W.) is grateful to the department of Physics and Astronomy at the University of Glasgow, where some of this work was done. We wish to thank Andrey Shirokov for useful discussions.

APPENDIX A: JOST FUNCTION ZEROS AND RESONANCE PHENOMENA

There does not appear to be any universally accepted definition of ''resonance phenomena'' in scattering theory. Experimenters may consider any sharp peak in a cross section to be a resonance. Theorists usually associate resonances with complex poles of the S matrix, or equivalently (in potential scattering) with complex zeros of the Jost function. However, not every Jost function zero is properly associated with a resonance. Thus the Jost function for the well behaved potentials studied in Newton's classic book [17] has infinitely many complex zeros yet the scattering cross section may not display any resonances at all. According to Newton, a ''true resonance'' must be associated with a *well isolated* zero of the Jost function, and be such that the scattering phase shift increases from near zero to near π, passing rapidly through $\pi/2$, as the wave number (or the energy) passes through the resonance region [18]. The cross section near resonance is then well approximated by the Breit-Wigner formula. This is usually regarded as a consequence of the unitarity of the S matrix, and Weinberg [21] has recently given a clear presentation of the argument in the context of multichannel scattering in particle physics. However, the argument from unitarity involves an additional assumption that appears never to be seriously challenged, namely that the phase shift is small for wave numbers close to but still outside the resonance region. This assumption is false for the potential $V_{\rm cutoff}(r)$ of Eq. (8).

In this appendix we present the modified version of the unitarity argument, which is appropriate for the present paper. We present the discussion in the context of single channel s-wave scattering, but the extension to other partial waves and to multiple channel processes is straightforward.

The single channel S matrix is related to the Jost function through

$$S(k)\equiv e^{2i\delta(k)}=\frac{\mathfrak{F}^*(k)}{\mathfrak{F}(k)}, \tag{A1}$$

where $\delta(k)$ is the scattering phase shift. Now suppose that

$$\mathfrak{F}(k)=\left(k-K+\frac{1}{2}i\Gamma\right)F(k). \tag{A2}$$

Then $\delta(k)$ can be written as

$$\delta(k)=\delta_{\rm r}(k)+\delta_{\rm nr}(k), \tag{A3}$$

where the ''resonant'' contribution to the phase shift, $\delta_{\rm r}(k)$, is given by

$$e^{2i\delta_{\rm r}(k)}=\frac{k-K-\frac{1}{2}i\Gamma}{k-K+\frac{1}{2}i\Gamma}, \tag{A4}$$

or equivalently

$$e^{i\delta_{\rm r}(k)}=\frac{k-K-\frac{1}{2}i\Gamma}{\left|k-K+\frac{1}{2}i\Gamma\right|}, \tag{A5}$$

and the ''nonresonant'' contribution, $\delta_{\rm nr}(k)$, by

$$e^{2i\delta_{\rm nr}(k)}=\frac{F^*(k)}{F(k)} \tag{A6}$$

[Weinberg [21] uses δ_{0N} for a ''nonresonant'' phase shift equivalent to our $\delta_{\rm nr}(k)$]. We suppose that the zero $k=K-\frac{1}{2}i\Gamma$ is well isolated, in the sense that if $K'-\frac{1}{2}i\Gamma'$ is any other zero of $F(k)$, then $\Gamma\ll[(K-K')^2+(\Gamma-\Gamma')^2]^{1/2}$. Equation (A5) then shows that as k increases through real values from $k\ll K$ to $k\gg K$, the resonant contribution to the

phase shift increases rapidly through $\pi/2$, while Eq. (A6) together with the postulated isolation of the zero at $K-\frac{1}{2}i\Gamma$ shows that the nonresonant contribution changes relatively slowly near $k=K$. We therefore make the approximation $\delta_{\rm nr}(k)\approx\text{const}=\delta_{\rm nr}(K)$ when k is close to K.

Now

$$\sin^2\,\delta(k)=\tfrac{1}{4}\left|e^{2i\delta(k)}-1\right|^2. \tag{A7}$$

In the usual resonance situation, the nonresonant phase shift is small as well as slowly varying in the resonant region. In this case, the approximation $\delta_{\rm nr}(k)\approx\delta_{\rm nr}(K)\approx 0$ leads to the conventional Breit-Wigner formula

$$\sin^2\delta(k)\approx\frac{\frac{1}{4}\Gamma^2}{(k-K)^2+\frac{1}{4}\Gamma^2},\quad \delta_{\rm nr}(K)\approx 0. \tag{A8}$$

However, neither the unitarity of the S matrix nor the isolation of the Jost function zero requires that $\delta_{\rm nr}(K)\approx 0$. If $\delta_{\rm nr}(K)=\pm\pi/2$, then

$$\sin^2\,\delta(k)\approx 1-\frac{\frac{1}{4}\Gamma^2}{(k-K)^2+\frac{1}{4}\Gamma^2}=\frac{(k-K)^2}{(k-K)^2+\frac{1}{4}\Gamma^2},$$

$$\delta_{\rm nr}(K)\approx\pm\frac{\pi}{2}, \tag{A9}$$

and the cross section is zero when $k=K$, at the ''peak'' of the ''inverted Breit-Wigner'' shape.

This last example is an extreme case of the Ramsauer-Townsend effect (see p. 165 of Ref. [21]). In general, if $\delta_{\rm nr}(k)$ is slowly varying but not particularly close to zero, the cross section will vanish at some point $k=k_0\neq K$. This implies that

$$\delta_{\rm nr}(k_0)=\arctan\left(\frac{\frac{1}{2}\Gamma}{k_0-K}\right). \tag{A10}$$

If $k_0\approx K$, then we make the approximation $\delta_{\rm nr}(k)\approx\delta_{\rm nr}(K)\approx\delta_{\rm nr}(k_0)$ to find

$$\sin^2\,\delta(k)\approx\frac{\frac{1}{4}\Gamma^2}{(k-K)^2+\frac{1}{4}\Gamma^2}\,\frac{(k-k_0)^2}{(k_0-K)^2+\frac{1}{4}\Gamma^2}. \tag{A11}$$

Thus the general Ramsauer-Townsend effect modulates the Breit-Wigner shape with the additional factor $(k-k_0)^2/[(k_0-K)^2+\frac{1}{4}\Gamma^2]$. We refer to Eq. (A11) as the ''pole approximation.'' Since Eq. (A11) is an approximation to $\sin^2\delta(k)$ associated with a well isolated zero of the Jost function, and since in this approximation the total phase shift increases rapidly from near $\delta_{\rm nr}(k_0)$ to near $\delta_{\rm nr}(k_0)+\pi$ as k increases past K, we regard Eq. (A11) as representing a generalized ''resonance phenomenon.'' Extreme examples of this phenomenon were encountered in Sec. IV and V, and were illustrated in Figs. 1 and 2.

APPENDIX B: THE PHASE SHIFT NEAR RESONANCE

In this appendix, we justify the assertions made in Sec. IV that the phase shift near $k=k_0$ increases rapidly from near $-\pi/2$ to near $+\pi/2$, but never reaches $+\pi/2$ and reaches $-\pi/2$ only if $\lambda\lesssim 27/(16n\pi)$. If $\delta(k,a)=\pm\pi/2$ then $\mathrm{Re}\mathfrak{F}(k,a)=0$. More generally, the phase shift will be close to $\pm\pi/2$ if $|\mathrm{Im}\mathfrak{F}(k,a)|\gg|\mathrm{Re}\mathfrak{F}(k,a)|$. We therefore study $\mathrm{Re}\mathfrak{F}(k,a)$ and $\mathrm{Im}\mathfrak{F}(k,a)$ close to $k=k_0$.

For convenience we define

$$\xi=(k-k_0)a=ka-n\pi. \tag{B1}$$

From this definition and Eq. (16),

$$\mathrm{Re}\mathfrak{F}(k,a)=1-\frac{2n^3\pi^3\,\sin 2\xi}{\xi(\xi+n\pi)(\xi+2n\pi)(\lambda+2n\pi)} \tag{B2}$$

and

$$\mathrm{Im}\mathfrak{F}(k,a)=-\frac{2n^3\pi^3(1-\cos 2\xi)}{\xi(\xi+n\pi)(\xi+2n\pi)(\lambda+2n\pi)}. \tag{B3}$$

We expand $\mathrm{Re}\mathfrak{F}(k,a)$ and $\mathrm{Im}\mathfrak{F}(k,a)$ as a power series in ξ, retaining terms up to order ξ^2 and using $n\pi\gg 1$ to simplify the coefficients where appropriate. This yields

$$\mathrm{Re}\mathfrak{F}(k,a)\approx\frac{1}{\lambda+2n\pi}\left(\lambda+3\xi+\frac{4n\pi}{3}\xi^2\right) \tag{B4}$$

and

$$\mathrm{Im}\mathfrak{F}(k,a)\approx\frac{1}{\lambda+2n\pi}(-2n\pi\xi+3\xi^2). \tag{B5}$$

Hence near $\xi=0$,

$$\tan\delta(k,a)\equiv-\frac{\mathrm{Im}\mathfrak{F}(k,a)}{\mathrm{Re}\mathfrak{F}(k,a)}\approx\frac{6n\pi\xi-9\xi^2}{3\lambda+9\xi+4n\pi\xi^2}. \tag{B6}$$

This has extrema when $\xi=\xi_\pm$ with

$$\xi_\pm=\frac{1}{8n^2\pi^2+27}(-9\lambda\pm\sqrt{81\lambda^2+48n^3\pi^3\lambda+162n\pi\lambda})$$

$$\approx\pm\frac{1}{2}\sqrt{\frac{3\lambda}{n\pi}}, \tag{B7}$$

where we have assumed $n\pi\gg\lambda$ and $n\pi\gg 1$ to obtain the final result. The corresponding extrema are

$$[\tan\,\delta(k,a)]_\pm\approx\pm\frac{1}{2}\sqrt{\frac{3n\pi}{\lambda}}. \tag{B8}$$

Provided that $n\pi\gg\lambda$, this justifies the assertion that the phase shift increases rapidly from close to $-\pi/2$ (when $\xi\approx\xi_-$) to near $+\pi/2$ (when $\xi\approx\xi_+$) as k increases through k_0 (or equivalently as ξ increases through zero).

From Eq. (B4), the zeros of $\mathrm{Re}\mathfrak{F}(k,a)$ near $k=k_0$ (or $\xi=0$) are at

$$\xi=-\frac{9}{8n\pi}\left[1\pm\sqrt{1-\frac{16n\pi\lambda}{27}}\right],$$

or equivalently

$$k_{\pm}=k_0-\frac{9}{8n\pi a}\left[1\pm\sqrt{1-\frac{16n\pi\lambda}{27}}\right]. \tag{B9}$$

These are real only for $\lambda\leqslant 27/(16n\pi)$, and if this is true, then the zeros $k_{\pm}$ are both smaller than k_0 so that $\tan\delta(k,a)<0$ for k near $k_{\pm}$. This justifies the claim that $\delta(k,a)$ never reaches $+\pi/2$ near $k=k_0$, and reaches $-\pi/2$ only if $\lambda\lesssim 27/(16n\pi)$.

APPENDIX C: IMAGINARY ZEROS OF THE JOST FUNCTION

In this appendix we justify the account of the imaginary zeros of the Jost function given in Sec. VI. We begin with Eq. (37).

The function $f(y)\equiv y/(1-e^{-2y})$ is positive definite, approaches zero exponentially as $y\to-\infty$, approaches y exponentially as $y\to\infty$, and is always greater than y. The quadratic function $D(y)$ is positive definite provided $\lambda+2b>1.6$. The linear function $N(y)$ changes sign when $y=y_0(\beta)$, where

$$y_0(\beta)=-b\,\frac{(\lambda+2b)\cos 2\beta-\sin 2\beta}{(\lambda+2b)\sin 2\beta-2(1-\cos 2\beta)}. \tag{C1}$$

The function $y_0(\beta)$ increases monotonically with β. At the sign change, $N(y)$ is increasing or decreasing accordingly as $(\lambda+2b)\sin 2\beta-2(1-\cos 2\beta)$ is positive or negative, respectively: in particular, $-bN(y)/D(y)$ has the same sign as $(\lambda+2b)\sin 2\beta-2(1-\cos 2\beta)$ for large negative y, and the opposite sign for large positive y. As $y\to\pm\infty$, the ratio $-bN(y)/D(y)$ approaches zero as the inverse first power of y.

From Eq. (C1), $\lim_{\beta\to 0}y_0(\beta)=-\infty$. As β increases, so also does $y_0(\beta)$, reaching infinity when $\beta=\arctan[\frac{1}{2}(\lambda+2b)]$. As β continues to increase, $y_0(\beta)$ starts out again from $-\infty$ and continues to increase, approaching $+\infty$ again as $\beta\to\pi$.

It follows from these remarks that $-bN(y)/D(y)<0$ for $0<\beta<\arctan[\frac{1}{2}(\lambda+2b)]$ and $y>y_0(\beta)$. Since $y/(1-e^{-2y})>0$, it follows that Eq. (37) has only one solution $y_1(\beta)$ for $0<\beta<\arctan[\frac{1}{2}(\lambda+2b)]$, which satisfies $y_1(\beta)<y_0(\beta)$. Hence, $y_1(0)=-\infty$. As β increases, $y_1(\beta)$ follows $y_0(\beta)$ along the y axis. If $\beta>\arctan[\frac{1}{2}(\lambda+2b)]$, then $-bN(y)/D(y)<0$ for $y<y_0(\beta)$ and $-bN(y)/D(y)>0$ for $y>y_0(\beta)$. Hence, a second zero $y_2(\beta)$ satisfying $y_0(\beta)<y_2(\beta)<y_1(\beta)$ starts moving from $-\infty$ along the y axis as β increases beyond $\arctan[\frac{1}{2}(\lambda+2b)]$. This qualitative behavior is illustrated in Fig. 3.

Near $y=0$ we make the approximations $b\gg 1$ and $b\gg|y|$ to find

$$\frac{bN(y)}{D(y)}\approx\frac{2b\,\cos 2\beta+2y\,\sin 2\beta}{\lambda+2b}, \tag{C2}$$

where we retain the term linear in y in case $|\cos 2\beta|\lesssim 1/2b$. The quadratic approximation

$$\frac{y}{1-e^{-2y}}\approx\frac{1}{2}+\frac{1}{2}y+\frac{1}{6}y^2 \tag{C3}$$

is extremely good for $-1\leqslant y\leqslant 1$ and fair even for $y=\pm 1.5$. Thus near $y=0$ we use these approximations, Eqs. (C1) and (C2), together with $b\gg 1$ in Eq. (37) to find

$$y^2+3y+3+\frac{12b\,\cos 2\beta}{\lambda+2b}=0. \tag{C4}$$

This quadratic equation has roots

$$y_{1,2}=-\frac{3}{2}\pm\sqrt{-\frac{3}{4}-\frac{12b\,\cos 2\beta}{\lambda+2b}}, \tag{C5}$$

but since the approximation Eq. (C3) is inadequate for $y<-1$, the root y_2, with negative sign in Eq. (C5), is unreliable as a solution of Eq. (37), and should not even exist if $\beta<\arctan[\frac{1}{2}(\lambda+2b)]$. For $\beta>\arctan[\frac{1}{2}(\lambda+2b)]$, the true second root y_2 will lie somewhere between $y_0(\beta)$ and the estimate given by Eq. (C5).

The root y_1, with positive sign in Eq. (C5), should be reliable provided it is greater than or equal to -1. This will be so provided

$$\begin{aligned}0.28\pi<\frac{1}{2}\arccos\left(-\frac{\lambda+2b}{12b}\right)\leqslant\beta\\ \leqslant\pi-\frac{1}{2}\arccos\left(-\frac{\lambda+2b}{12b}\right)<0.72\pi.\end{aligned} \tag{C6}$$

However, when $\beta\approx\frac{1}{2}\arccos[-(\lambda+2b)/4b]\approx\pi/3$ there is a near cancellation in Eq. (C5) so that the approximations made in its derivation become suspect. In this case a better approximation is obtained using a linear approximation to $y/(1-e^{-2y})$, equivalent to ignoring the quadratic term in Eq. (C4). This yields

$$y_1\approx-1-\frac{4b\,\cos 2\beta}{\lambda+2b},\quad \beta\approx\frac{1}{2}\arccos\left(-\frac{\lambda+2b}{4b}\right). \tag{C7}$$

For the examples illustrated in Fig. 2, Eq. (C7) correctly predicts $y_1>0$ for $\beta=\pi/3$, yielding a bound state, while Eq. (C5) fails to do so.

The root y_1 reaches a maximum

$$y_{1\max}=-\frac{3}{2}+\sqrt{\frac{12b}{\lambda+2b}-\frac{3}{4}}\lesssim 0.79 \tag{C8}$$

when $\beta=\pi/2$. Since $y_{1\max}<1$, we expect this to be a reliable estimate provided the approximation $b\equiv k_0 a\gg 1$ is valid.

Equation (C5) predicts two real roots $y_{1,2}$ provided that

$$0.27\pi<\frac{1}{2}\arccos\left(-\frac{\lambda+2b}{16b}\right)\leqslant\beta \leqslant\pi-\frac{1}{2}\arccos\left(-\frac{\lambda+2b}{16b}\right)<0.73\pi. \tag{C9}$$

As we have already noted, the root y_2 is unreliable as a solution of Eq. (37), and does not exist for $\beta<\arctan[\frac{1}{2}(\lambda+2b)]$. However, Eq. (37) has either two roots or no roots for $\beta>\arctan[\frac{1}{2}(\lambda+2b)]$, which is close to $\pi/2$ when $b\gg 1$. Therefore, even though the numerical predictions for y_2 are unreliable, we may expect that Eq. (C5) will yield qualitatively useful information for β near $\beta_0\equiv\pi-\frac{1}{2}\arccos[-(\lambda+2b)/16b]$. We first note that for $\beta=\beta_0$ and $b\gg 1$,

$$y_0(\beta_0)\approx -b\ \cot 2\beta_0<-\frac{\lambda+2b}{16}. \tag{C10}$$

From this, $y_0(\beta_0)<y_2$, and Eq. (C5) we expect that when $\beta\approx\beta_0$ the two roots will coincide with $-(\lambda+2b)/16\lesssim y_1=y_2\lesssim -1.5$, while for larger β they will separate and move into the complex y plane with equal and opposite imaginary parts. In terms of the wave number $k=iy/a$, the imaginary zeros of the Jost function will coalesce for $\beta\approx\beta_0$ and then separate, moving into the complex k plane with equal and opposite real parts as β increases past β_0.

[1] J. von Neumann and E. Wigner, Phys. Z. **30**, 465 (1929).

[2] T. Cowan *et al.*, Phys. Rev. Lett. **56**, 444 (1986); P. Salabura *et al.*, Phys. Lett. B **245**, 153 (1990); W. Kroenig *et al.*, *ibid.* **218**, 12 (1989); Z. Phys. A **246**, 153 (1993).

[3] J. R. Spence and J. P. Vary, Phys. Lett. B **254**, 1 (1990).

[4] B. A. Arbuzov *et al.*, in *Problems of High Energy Physics and Field Theory*, edited by V. A. Petrov (Nauka, Moscow, 1989), p. 362; Mod. Phys. Lett. A **5**, 1441 (1990).

[5] F. Capasso, C. Sirtori, J. Faist, D. L. Sivco, S. G. Chu, and A. Y. Cho, Nature (London), Phys. Sci. **358**, 565 (1992).

[6] T. A. Weber, Solid State Commun. **90**, 713 (1994).

[7] B. A. Arbuzov, E. E. Boos, V. I. Savrin, and S. A. Shichanin, Pis'ma Zh. Eksp. Teor. Fiz. **50**, 236 (1989) [JETP Lett. **50**, 262 (1989)]; B. A. Arbuzov, S. A. Shichanin, and V. I. Savrin, Phys. Lett. B **275**, 144 (1992).

[8] T. A. Weber and D. L. Pursey, Phys. Lett. B **331**, 430 (1994).

[9] L. G. Zastavenko, Preprint, Joint Inst. Nucl. Res., Dubna, USSR **53**, 9 (1992).

[10] D. L. Pursey and T. A. Weber, Phys. Rev. A **52**, 3932 (1995).

[11] T. A. Weber and D. L. Pursey, Phys. Rev. A **50**, 4478 (1994); D. L. Pursey and T. A. Weber, *ibid.* **50**, 4472 (1994).

[12] J. Pappademos, U. Sukhatme, and A. Pagnamenta, Phys. Rev. A **48**, 3525 (1993).

[13] A. A. Stahlhofen, Phys. Rev. A **51**, 934 (1995).

[14] G. Darboux, C. R. Acad. Sci. **94**, 1456 (1882).

[15] T. Regge, Nuovo Cimento **8**, 671 (1958).

[16] D. L. Pursey and T. A. Weber, Phys. Rev. A **52**, 4255 (1995).

[17] See for example, Roger G. Newton, *Scattering Theory of Waves and Particles*, 2nd ed. (Springer-Verlag, New York, 1982), Chap. 12.

[18] T. A. Weber, C. L. Hammer, and V. S. Zidell, Am. J. Phys. **50**, 839 (1982).

[19] H. Dehnen and M. Shahin, Acta Phys. Pol. B **21**, 477 (1990).

[20] T. A. Weber, in *Proceedings of XIth International Workshop on Quantum Field Theory and High Energy Physics*, edited by B. B. Levchenko (Moscow State University, Moscow, 1997), p. 419.

[21] Steven Weinberg, *The Quantum Theory of Fields* (Cambridge University Press, Cambridge, 1995), Vol. 1, pp. 159–165.